An actuated elastic sheet interacting with passive and active structures in a viscoelastic fluid

J. C. Chrispell, L. J. Fauci, and M. Shelley

Citation: Phys. Fluids **25**, 013103 (2013); doi: 10.1063/1.4789410
View online: http://dx.doi.org/10.1063/1.4789410
View Table of Contents: http://pof.aip.org/resource/1/PHFLE6/v25/i1
Published by the American Institute of Physics.

PHYSICS OF FLUIDS **25**, 013103 (2013)

An actuated elastic sheet interacting with passive and active structures in a viscoelastic fluid

J. C. Chrispell,[1,a)] L. J. Fauci,[2,b)] and M. Shelley[3]
[1]*Department of Mathematics, Indiana University of Pennsylvania, Indiana, Pennsylvania 15705, USA*
[2]*Department of Mathematics, Tulane University, New Orleans, Louisiana 70118, USA*
[3]*Applied Mathematics Lab, The Courant Institute, New York University, New York City, New York 10012, USA*

(Received 16 May 2012; accepted 3 December 2012; published online 31 January 2013)

We adapt the classic Taylor swimming sheet set-up to investigate both the transient and long-time dynamics of an actuated elastic sheet immersed in a viscoelastic fluid as it interacts with neighboring structures. While the *preferred* kinematics of the sheet are specified, the flexible sheet interacts with the surrounding fluid and other structures, and its realized kinematics emerges from this coupling. We use an immersed boundary framework to evolve the Oldroyd-B/Navier-Stokes equations and capture the spatial and temporal development of viscoelastic stresses and sheet shape. We compare the dynamics when the actuated sheet swims next to a free elastic membrane, with and without bending rigidity, and next to a fixed wall. We demonstrate that the sheets can exploit the neighboring structures to enhance their swimming speed and efficiency, and also examine how this depends upon fluid viscoelasticity. When the neighboring structure is likewise an actuated elastic sheet, we investigate the viscoelastic dynamics of phase-locking. © *2013 American Institute of Physics*. [http://dx.doi.org/10.1063/1.4789410]

I. INTRODUCTION

The analysis of the fluid dynamics of flagellated microorganisms was initiated in the classic paper of Taylor[1] where the swimming of an infinite sheet undergoing small sinusoidal oscillations in a Stokesian fluid was studied. This simple model elucidated some of the basic features of flagellar motility such as the quadratic dependence of swimming speed and linear dependence of energy dissipation upon the wave amplitude. It was also shown that the minimal energy configuration of two parallel sheets was achieved for in-phase beating. In the decades since, there has been an explosion in analytical, computational, and experimental investigations[2] that have demonstrated both unifying principles of the fluid dynamics of microorganism motility, as well as the diversity of properties only possible when details of individual systems are accounted for.

The classical swimming sheet set-up has been used as a testbed to examine a variety of fundamental issues in microorganism fluid dynamics such as the effect of walls[3] and the effect of non-Newtonian fluid environments[4–6] on motility properties. Early computational studies demonstrated that the dynamic phase-locking of flexible neighboring sheets was achieved by an emergent time-dependent difference in swimming velocities.[7] More recently, analytical studies of phase-synchronization of sheets both in a Newtonian fluid[8,9] and a viscoelastic fluid[10] have been presented.

A microorganism's undulating flagellum rarely beats freely, but interacts with other flagella, either from the same cell or those of nearby cells. In addition, a flagellum may beat in close proximity to passive elastic structures such as mucosal strands in the surrounding fluid or other cell appendages. The ventral flagella of the intestinal parasite *Giardia* beat in a region bounded by ventral flanges

[a)]Author to whom correspondence should be addressed. Electronic mail: john.chrispell@iup.edu.
[b)]Also at Center for Computational Science, Tulane University, New Orleans, Louisiana 70118, USA.

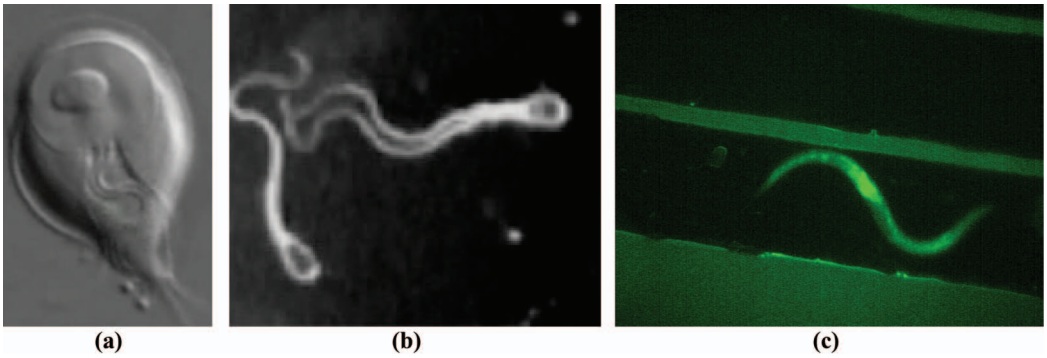

FIG. 1. (a) The ventral flagella of the intestinal parasite *Giardia* beat in a region bounded by ventral flanges. Reproduced with permission from S. A. House, D. J. Richter, J. K. Pham, and S. C. Dawson, PLoS Pathog. **7**(8), e1002167 (2011). Copyright 2011 PLOS. (b) Synchronization in bull spermatozoa. Reproduced with permission from D. Woolley, R. Crockett, W. Groom, and S. Revell, J. Exp. Biol. **212**, 2215 (2009). Copyright 2009 The Company of Biologists. (c) A *Caenorhabditis elegans* swimming in a restricted channel (photo courtesy of Applied Mathematics Lab, Courant Institute).

(Figure 1(a)).[11] These flagella have been implicated in the attachment of this microbe to intestinal microvilli. Woolley *et al.*[12] recently demonstrated flagellar synchronization in bull spermatozoa in experiments where the swimming was confined to a glass surface. After rapidly synchronizing their beatforms, the two flagella are attracted to each other and become almost conjoined (Figure 1(b)).

Caenorhabditis elegans is a model organism that swims due to undulatory waves passed along its body. While the Reynolds number of its swimming is close to one, the fluid dynamics governing motility remain dominated by viscous forces.[13] Nematodes such as *C. elegans* often swim in restricted environments such as saturated soils. Understanding the effect of nearby structures on the dynamics of this swimming has been the subject of recent experiments and theoretical investigations.[14,15] Figure 1(c) shows a snapshot of a *C. elegans* swimming in a channel whose height is smaller than the length of the undulator.

In this paper we adapt the classic Taylor swimming sheet set-up to investigate the transient and long-time dynamics when an actuated elastic sheet immersed in a viscoelastic fluid interacts with neighboring structures. While the *preferred* kinematics of the sheet are specified, the flexible sheet interacts with the surrounding fluid, and other structures, and its realized kinematics emerges from this coupling. We will examine the coupled system when this neighboring structure is a fixed wall or a free elastic membrane with and without bending rigidity. We will demonstrate that the sheets can exploit the neighboring structures to enhance their swimming speed and efficiency, and also examine how this depends upon fluid viscoelasticity.

We also examine the case when the neighboring structure is likewise an actuated elastic sheet, and investigate the viscoelastic fluid dynamics of phase-locking. It is important to note that in the zero-Reynolds number Newtonian case, two neighboring sheets oscillating with prescribed sinusoidal kinematics cannot phase-lock due to considerations of symmetry and time-reversal.[8] In contrast, three symmetry-breaking effects are in play in the system presented here—the viscoelasticity of the fluid, the elasticity of the flexible sheets, and the small, but non-zero, inertia of the fluid. The effect of viscoelasticity alone on phase-locking was examined in Ref. 10 in the limit of small amplitude, kinematically prescribed sinusoidal shapes. In addition, the effect of sheet elasticity alone on phase-locking was examined in Ref. 16 where it was demonstrated that in a zero-Reynolds number Newtonian fluid the interaction within the fluid/elastic-sheet system gave rise to modulations of sheet amplitudes. Below we will also demonstrate a similar dynamic modulation of sheet amplitudes in an Oldroyd-B/Navier-Stokes fluid.

II. MODEL

We explore the interaction between two elastic sheets Γ_1 and Γ_2 immersed in a two-dimensional domain Ω filled with a viscoelastic fluid. Periodic boundary conditions are used to achieve their

infinite extent. Each of these sheets are endowed with elastic properties and one or both will also be actuated.

As in Refs. 7 and 17, each sheet is taken to be a generalized Euler elastica whose elastic energy is composed of a tensile and an active bending component. The tensile energy of the lth sheet $l = 1$, 2 (whose position is given by $\boldsymbol{X}_l(s,t)$) is

$$\mathcal{E}_{tens,l} = \frac{S_{I,l}}{2}\int_0^1 \left(\left\|\frac{\partial \boldsymbol{X}_l}{\partial s}\right\| - 1\right)^2 ds. \tag{1}$$

The stiffness or penalty parameter $S_{I,\,l}$ is chosen large enough to control excessive extension or compression. The bending energy for each sheet is given by

$$\mathcal{E}_{bend,l} = \frac{S_{c,l}}{2}\int_0^1 (\kappa_l(s,t) - \hat{\kappa}_l(s,t))^2 ds. \tag{2}$$

Here $\hat{\kappa}_l$ is a specified target curvature. If this target curvature is set to zero, the sheet is not actuated, but resists bending. Conversely, when this target curvature is chosen to be an appropriate function of position and time, the now-actuated sheet pursues a traveling wave of specified kinematics. Because the sheet will be coupled to the surrounding viscoelastic fluid, these kinematics will be only approximately achieved. How close the realized kinematics are to the preferred kinematics is governed by the choice of the bending stiffness parameter $S_{c,\,l}$.

The force that the lth immersed sheet exerts on the surrounding fluid is derived from these energies:

$$\boldsymbol{F}_l(s,t) = -\frac{\delta}{\delta \mathbf{X}_l}\left(\mathcal{E}_{tens,l} + \mathcal{E}_{bend,l}\right). \tag{3}$$

We choose an Oldroyd-B/Navier-Stokes description of the viscoelastic fluid.[18,19] The governing equations, written in adimensional form, are

$$Re\frac{D\boldsymbol{u}}{Dt} + \nabla p - (1-\alpha)\Delta \boldsymbol{u} - \nabla\cdot\boldsymbol{\sigma} = \mathbf{f} \text{ in } \Omega, \tag{4}$$

$$\boldsymbol{\sigma} + De\boldsymbol{\sigma}^{\nabla} - \alpha\left(\nabla\boldsymbol{u} + (\nabla\boldsymbol{u})^T\right) = \mathbf{0} \text{ in } \Omega, \tag{5}$$

$$\nabla\cdot\boldsymbol{u} = 0 \text{ in } \Omega. \tag{6}$$

Here the $\boldsymbol{u}$ is the fluid velocity, p is the pressure and $\boldsymbol{\sigma}$ is the extra stress generated by the transport and distension of an immersed polymer field. The material derivative and the upper convective derivative are defined as $\frac{D\boldsymbol{u}}{Dt} \equiv \frac{\partial \boldsymbol{u}}{\partial t} + \boldsymbol{u}\cdot\nabla\boldsymbol{u}$ and $\boldsymbol{\sigma}^{\nabla} \equiv \frac{D\boldsymbol{\sigma}}{Dt} - \left(\nabla\boldsymbol{u}\boldsymbol{\sigma} + \boldsymbol{\sigma}(\nabla\boldsymbol{u})^T\right)$, respectively. From the kinetic theory that underlies the Oldroyd-B model,[19] the related stress tensor $\tilde{\boldsymbol{\sigma}} = \frac{De}{\alpha}\boldsymbol{\sigma} + I$ measures the average distension of the polymer field and is also a positive semi-definite rank-two tensor.

The force of the elastic sheets on the fluid is represented by a Dirac delta layer of force supported along each sheet:

$$\mathbf{f}(\boldsymbol{x},t) = \sum_l \int_0^1 \boldsymbol{F}_l(s,t)\delta(\boldsymbol{x} - \boldsymbol{X}_l(s,t))\, ds. \tag{7}$$

The Reynolds number Re and the Deborah number De are defined by

$$Re = \frac{LV\rho}{\mu_0} \quad \text{and} \quad De = \frac{\tau_p}{\tau_f}.$$

Here ρ is the fluid density, $\mu_0 = \mu_p + \mu_s$ is the total viscosity due to both polymer and solvent, L is the spatial period of the sheet, V is the speed of the bending wave, $\tau_f = L/V$, τ_p is the polymer relaxation time, and $\alpha = \mu_p/\mu_0$. Note that when $De = 0$ and $\alpha = 0$ the fluid is Newtonian.

The system is closed by imposing a no-slip condition for velocity at the immersed sheets:

$$\boldsymbol{u}(\boldsymbol{X}_l(s,t),t) = \frac{\partial \boldsymbol{X}_l(s,t)}{\partial t} = \int_\Omega \boldsymbol{u}(\boldsymbol{x},t)\delta(\boldsymbol{x} - \boldsymbol{X}_l(s,t))\, d\boldsymbol{x}. \tag{8}$$

This formulation of the coupled fluid-body system is readily discretized using an immersed boundary formulation,[20] where fluid quantities such as velocity, pressure, and polymer stress are tracked on a background Eulerian grid, while sheet related quantities such as elastic forces are treated in a Lagrangian manner. The use of grid-dependent discrete Dirac delta functions allows for the two-way coupling between the fluid and the sheets. Details of the numerical implementation of this Oldroyd-B/Navier-Stokes immersed boundary method are presented in Ref. 21 and the related Oldroyd-B/Stokes immersed boundary method in Ref. 22.

III. MODEL VALIDATION

While the swimming sheet problem is, itself, of fundamental interest in fluid mechanics, it also provides an excellent test problem for computational methods because of the availability of analytical results. We consider the sheet with the preferred kinematics,

$$y(s,t) = a + b\sin(\kappa s - \omega t), \tag{9}$$

where a is the center line of the sheet, b is its amplitude, κ is the wave number, and $V = \omega/\kappa$ is the wave speed.

An asymptotic expression for the swimming velocity U of the sheet as a function of its kinematics was first offered by Taylor[1] in the limit of small amplitude oscillations in a Newtonian fluid governed by the zero Reynolds number Stokes equations:

$$\frac{U}{V} = \frac{1}{2}b^2\kappa^2\left(1 - \frac{19}{16}b^2\kappa^2\right) + O(b^6\kappa^6). \tag{10}$$

Later, Tuck introduced a correction for non-zero Reynolds number:[23]

$$\frac{U}{V} = \frac{1}{4}b^2\kappa^2\left(1 + \frac{1}{F(Re)}\right) + O(b^4\kappa^4), \tag{11}$$

where

$$F(Re) = \left(\frac{1+\sqrt{1+Re^2}}{2}\right)^{\frac{1}{2}}.$$

Most recently, Lauga[4] considered the case of a viscoelastic fluid with non-zero Deborah number (De):

$$\frac{U}{V} = \left(\frac{1+De^2(1-\alpha)}{1+De^2}\right)\left(\frac{1}{2}b^2\kappa^2\right) + O(b^4\kappa^4).$$

Note that here $0 \le \alpha \le 1$ is the ratio of the polymer viscosity of the fluid to the total viscosity. This asymptotic result implies that the swimming velocity of the sheet is always greater in the Newtonian case $De = 0$.

In order to validate our Oldroyd-B/Navier-Stokes model where we are free to vary both Re and De, we choose the base parameters shown in Table I for a single swimming sheet. The continuous curves in Figure 2 show the asymptotic values of U/V for $Re = 0$, $De = 0$,[1] $Re = 1$, $De = 0$,[23] and $Re = 0$, $De = 1$.[4]

As described in Sec. II, while we specify the preferred kinematics of the sheet, the flexible elastic sheet does interact with the surrounding fluid and the realized kinematics emerge from this interaction. The discrete symbols in Figure 2 show the computed U/V as a function of the emergent amplitude of the swimming sheet. Due to the fact that we are solving the time-dependent Navier-Stokes equations coupled to an elastica, even in the low Reynolds number Newtonian case, the dynamics of the flow exhibit some transients. We record the overall swimming velocity U by averaging the horizontal velocity of immersed boundary points along the sheet and then average these values over the 16th–20th period of oscillation, when the system has achieved a steady state. The results in Figure 2 illustrate some very important points. The simulations of the Newtonian case for both $Re = 0.1$ and $Re = 1$ agree very well with both Taylor's and Tuck's small-amplitude

TABLE I. Base parameters for swimming sheet.

Parameter	Symbol	Value
Domain	Ω	$(0,1) \times (0,1)$
Background grid spacing	h	1/128
Time step	Δt	$1.25e-5$
Wave no.	κ	2π
Frequency	ω	2π
Curvature stiffness	S_c	50
Tensile stiffness	S_I	10 000

asymptotics.[1,23] As seen clearly in the inset of Figure 2, this agreement is better at smaller amplitudes. The simulations of the viscoelastic case $De = 1$ agree well with Lauga's asymptotics[4] at small amplitudes. Moreover, since the asymptotics assumed a Stokesian fluid $Re = 0$, the simulations for $Re = 0.1$ result in swimming speeds closer to the theory than those computed for $Re = 1$ (see inset of Figure 2).

In all simulations, periodic boundary conditions are imposed on each side of the rectangular domain. While these boundary conditions on the right and left enforce the infinite extent of the sheet, these conditions on the top and bottom of the domain can be interpreted as representing an infinite array of parallel swimmers. In order to determine if these periodic neighbors are influencing the dynamics, we performed simulations where the size of the computational "tank" was doubled. The results included in Figure 2 for the case $Re = 0.1$, $De = 1$ indicate that the domain is chosen large enough that the influence of periodic copies is negligible.

We remark that the asymptotic analysis and the simulations are based upon different physical scenarios. While it is impossible to quantify the contributions of each differing feature of the simulations and the asymptotics (e.g., non-zero inertia, non-exact sinusoidal kinematics, the influence

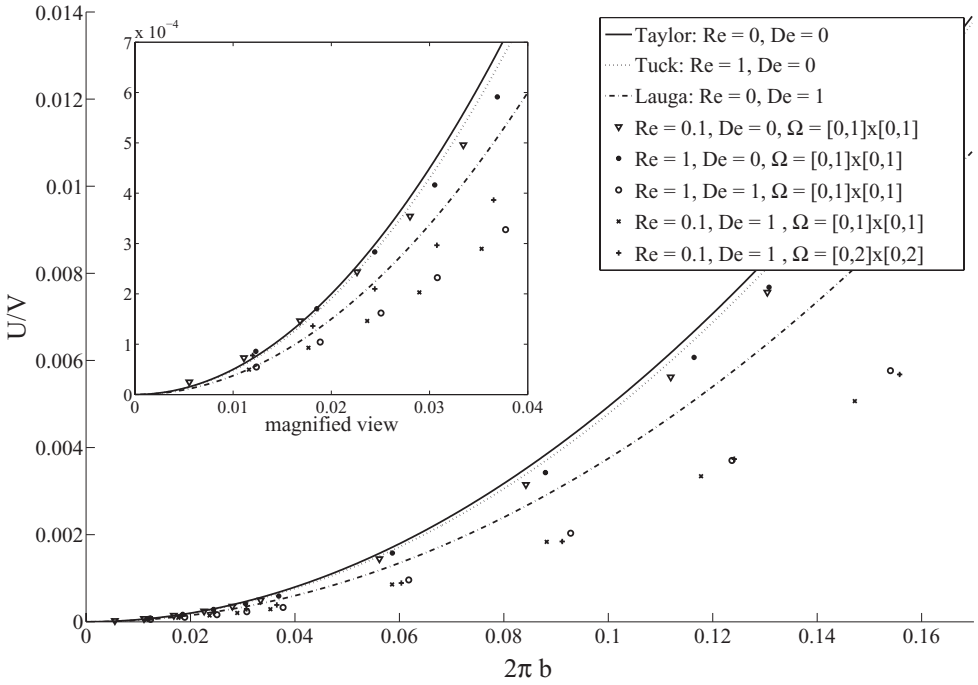

FIG. 2. The continuous curves show the asymptotic values of U/V for $Re = 0$, $De = 0$,[1] $Re = 1$, $De = 0$,[23] and $Re = 0$, $De = 1$.[4] The discrete symbols indicate the computed U/V when the Oldroyd-B/Navier-Stokes system was evolved at the indicated Re and De.

of periodic neighbors), it is important to perform numerical experiments that demonstrate convergence of the simulation solution as the background grid is refined. Convergence results of our Navier-Stokes/Oldroyd-B code have been reported previously for a related elastic interface problem.[21] In addition, we have simulated a single sheet (using $Re = 1$, $De = 1$, and $b = 0.025$) at three levels of grid refinement: 32×32, 64×64, and 128×128. The resulting sheet velocity, averaged over the second period of motion was 0.00490, 0.00609, and 0.00599, respectively. It is our conjecture that the differing physical assumptions underlying the asymptotics and the simulations lead to more differences in overall dynamics when fluid viscoelasticity is present.

IV. NUMERICAL RESULTS

Having calibrated our numerical method against known results, we now turn to the study of four other prototype situations, each of which involves an actuated sheet (or sheets) immersed in a viscoelastic fluid and interacting with another structure. These cases are summarized in Fig. 3 where the temporal evolution of these four systems are shown over 10 periods of actuation, starting from a state of zero polymer stress $\boldsymbol{\sigma}$. The first case (column 1) considers the swimming of two actuated sheets moving in the same direction but with their deformation waves initially out of phase. The second (column 2) examines an actuated sheet as it swims above and entrains a passive membrane under tension but with no bending rigidity ($S_{c,2} = 0$). The third (column 3) considers the same case but with the passive sheet having bending rigidity ($\hat{\kappa}_2 = 0$). Finally, the fourth (column 4) examines an actuated sheet as it swims above a fixed flat wall. Note that the first five rows in each column depict snapshots during the first two periods of actuation, while the last row shows the evolution after ten periods ($T = 10$).

A. The synchronization of two swimming sheets

Column 1 of Fig. 3 shows snapshots of the position of two actuated elastic sheets, immersed in a viscoelastic fluid, as they swim leftward through the rightward propagation of bending waves. Here $De = 1$. The initial deformation waves are $\pi/2$ out of phase with each other. The color field is the relative strain energy density, $tr\tilde{\boldsymbol{\sigma}}$, which gives the mean-squared distension of the polymer field.

The entire time-course of the dynamics shows that the two sheets move into alignment with each other, or synchronize, through a complex interaction of the sheet's internal mechanical stresses and those of the surrounding fluid. This tendency towards synchronization is quite dramatic during the first period of motion. During the synchronization process the top sheet initially swells in amplitude but eventually achieves a temporally constant amplitude (Fig. 4(a)). In contrast, the bottom sheet initially flattens with its amplitude then slowly approaches the same amplitude as the top sheet. (When simulations were performed for different bending rigidities of the sheets, we found that this terminal amplitude was an increasing function of the bending rigidity.)

There is initially no contribution from the polymer stress, it being initially zero, but as the sheets change shape and move relative to each other, polymer stress contributions quickly develop particularly within the first period. The details of this growth are shown in Fig. 5 which illustrates the distension of the polymer field by plotting ellipses whose axes are in the principle directions of the polymer conformation tensor $\tilde{\boldsymbol{\sigma}}$ and with these axes' lengths scaled by the corresponding eigenvalue. While the forward motion of the two sheets is quite small, very quickly large stresses develop due to the relative motion of the two sheets which is much more rapid. Of particular interest in its geometric form is the stress field at $t = 0.8$ which shows an arc of deformation that is typically associated with hoop stresses. As the sheets move into phase over a few cycles these stresses gradually relax to more moderate amplitudes which are maintained thereafter.

It is interesting to examine the temporally changing velocities and amplitudes of the two sheets. Figure 4(b) shows the velocity of each sheet over time. From an initial velocity set by their interaction through a pure Newtonian fluid, the velocities of the two sheets change on an apparent $O(De)$ time scale. Interestingly, while the top sheet shows a large increase in speed, the bottom sheet is actually

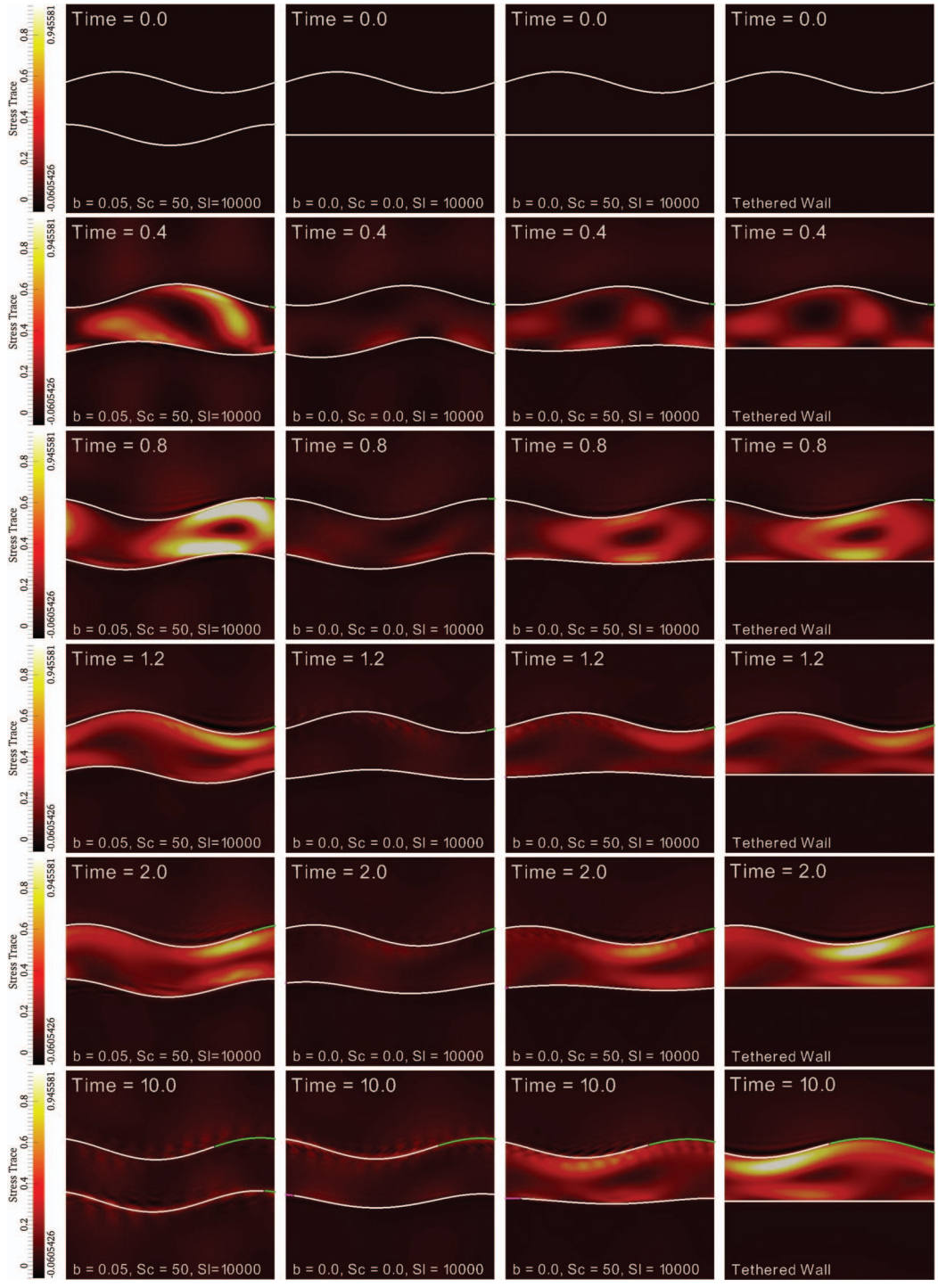

FIG. 3. Summary plot of four prototype problems of an actuated sheet swimming through a viscoelastic fluid ($De = 1$) and interacting with another immersed structure. Shown are snapshots of sheet positions over 10 periods of actuation, overlaid with the strain-energy density associated with the polymer conformation. In all cases the initial polymer stress is isotropic and uniform. Column 1: Two actuated sheets moving in the same direction but with their deformation waves initially out of phase. Column 2: An actuated sheet swimming above and entraining a passive membrane having no bending rigidity but under tension. Column 3: An actuated sheet swimming above a passive membrane with bending rigidity. Column 4: An actuated sheet swimming above a fixed flat wall.

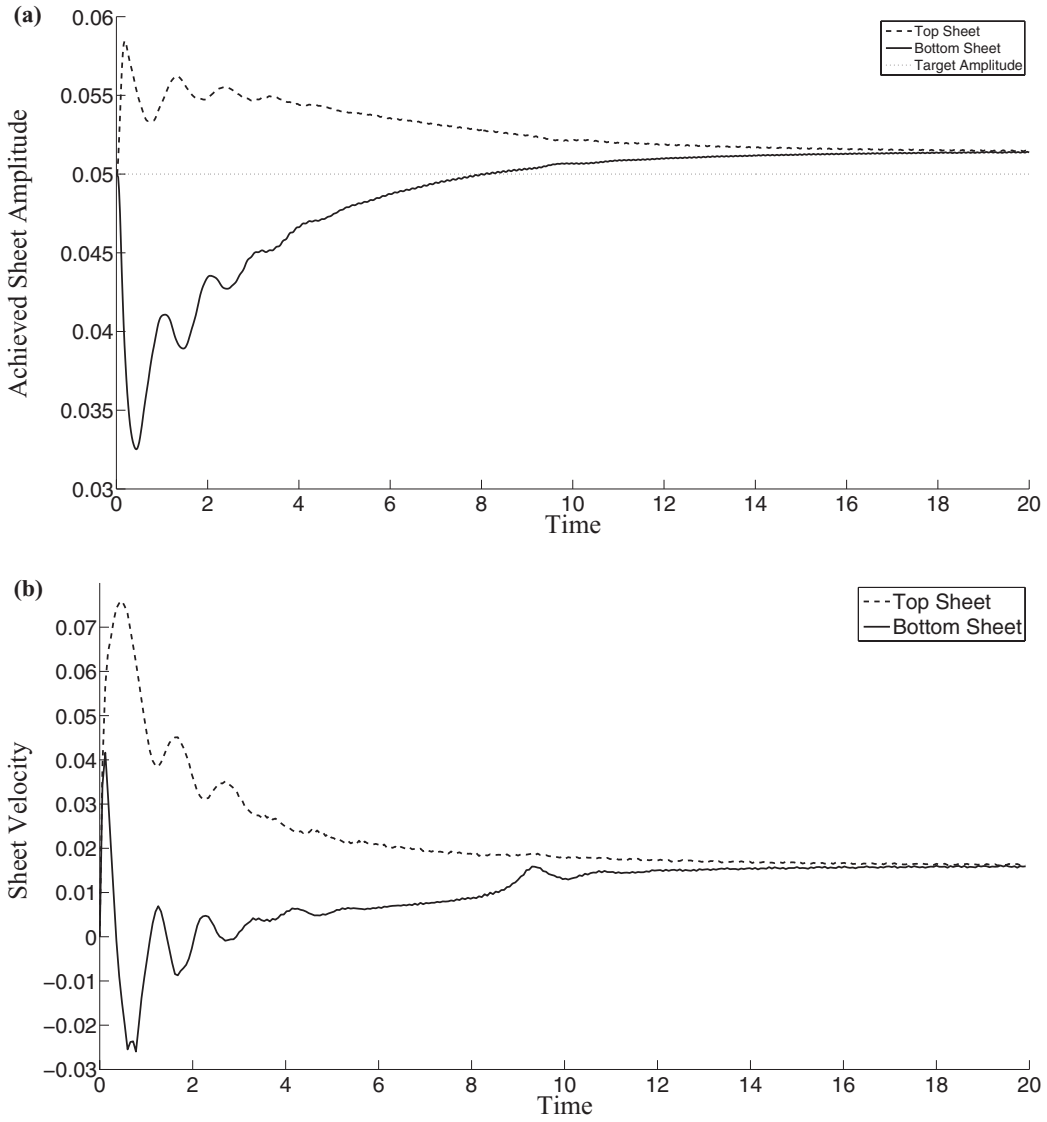

FIG. 4. (a) For $De = 1$, the temporal evolution of the achieved amplitudes of the top and bottom sheets. (b) The velocity of top and bottom sheets as they move into phase with each other. The two phase locking swimming sheets are initially configured $\pi/2$ (1/4 of a wavelength) out of phase with each other. The period of oscillation is $T = 1$.

pushed backward, and as suggested above the relative velocity between the two is nearly an order of magnitude larger than the terminal velocity. The approach to the terminal state is also quite slow, and is marked by oscillations. A signature of the very different speeds shown by the two sheets is found in Figure 4(a) which shows the wave amplitude of each as a function of time. The large initial velocity of the top sheet is correlated with an increase in wave amplitude, as is intuitively expected, and which again shows oscillations and a slow decay to a smaller sustained size. The bottom sheet, conversely, shows a large decrease in amplitude as it is pushed from above and backward by the more rapidly moving top sheet. The decrease in amplitude is over 30%. Note that the two sheets begin their evolution at amplitudes matched to the target amplitude of the internal curvature dynamics (shown as the dashed line at 0.05). This target amplitude is rapidly departed from, and is even slightly exceeded in the long-time dynamics.

We now examine the synchronization of the two sheets as the Deborah number alone is varied, using the same initial conditions as above. Figure 6 shows the swimming velocity of each sheet for

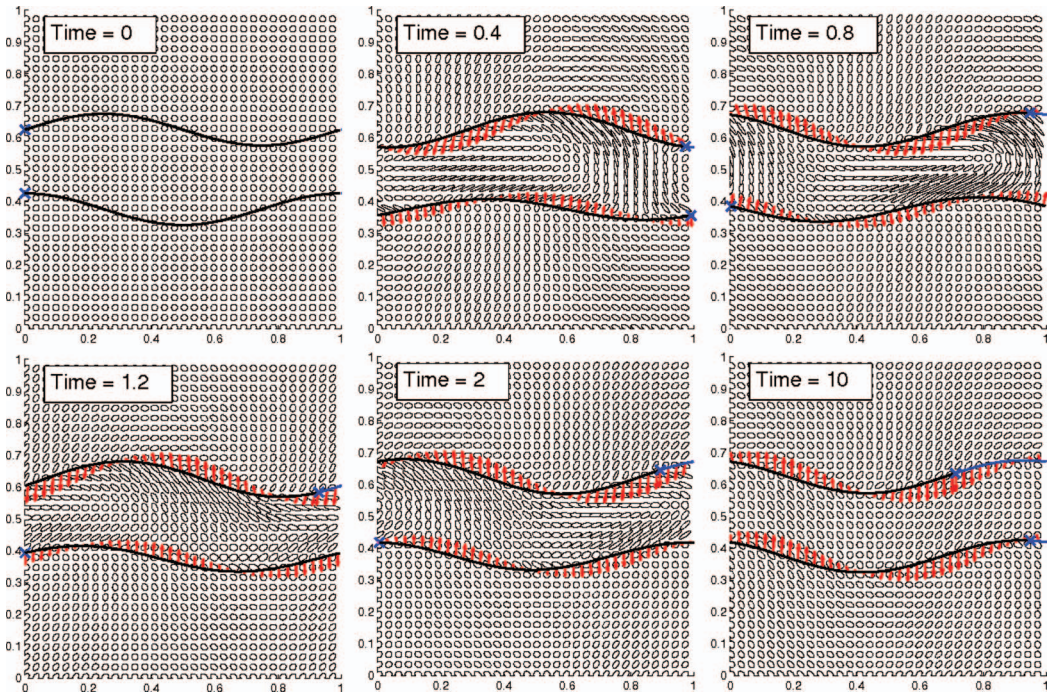

FIG. 5. Snapshots of two actuated sheets as they phase lock. The distension of the polymer field is visualized by ellipses whose axes are in the principle directions of the polymer conformation tensor $\tilde{\boldsymbol{\sigma}}$ with these axes' lengths scaled by the corresponding eigenvalue. Arrows along each filament indicate velocity, and the asterisks, originally placed at the leftmost material points on each filament at time zero, indicate material displacement. Note that the top sheet enjoyed considerably more translation than the bottom sheet.

various Deborah numbers *De*, and the detail of these dynamics for early time is shown in the inset. At each value, the top sheet moves quickly in its direction of desired propagation, while the bottom sheet's motion is hindered and pushed backward despite its own shape actuation. The initial transient behavior of the sheets that are started from rest in a uniform isotropic stress field indicate a dramatic boost towards synchronization that is most pronounced at the highest Deborah number, decreasing monotonically for smaller Deborah numbers (see inset of Figure 6). As the sheets progress, however, we see a reversal of this trend when we examine the times at which the swimming velocities of the two sheets synchronize. By this measure, the Newtonian sheets are the first to achieve synchrony, followed monotonically in Deborah number by the sheets swimming in viscoelastic fluids. This slow relaxation towards synchronization may also be measured by tracking the position of the upwardly concave critical points for each sheet. We consider the sheets to be phase locked once the distance between these points is less than a value of 3/4 of a mesh spacing. We denote this "time to phase lock" by T_{pl}, and plot these values in Fig. 7 as a function of Deborah number. Again, this plot indicates that time to phase-locking increases monotonically with the viscoelasticity of the fluid. This seems intuitively correct as in the infinite *De* limit, the viscoelastic fluid becomes a viscously damped hyperelastic solid.

These results, on their face, differ from the analytical predictions of Elfring *et al.*,[10] where they also study the synchronization of two actuated sheets immersed in an Oldroyd-B fluid. We caution that a direct comparison between these computational results and the analysis of Ref. 10 cannot be made given the very different physical scenarios that are hypothesized. The analysis, for zero-Reynolds number flow, is in the limit of small wave amplitude for sheets whose shapes are kinematically specified. The small amplitude analysis gives that synchronization should take place on an $O(\epsilon^{-2})$ time scale as opposed to the asymptotically slower $O(\epsilon^{-4})$ time scale of the Newtonian case. Our finding, for non-zero Reynolds number, is reversed with the Newtonian case being the fastest. Also, our simulations are not in the small-amplitude regime, nor are the sheet shapes specified

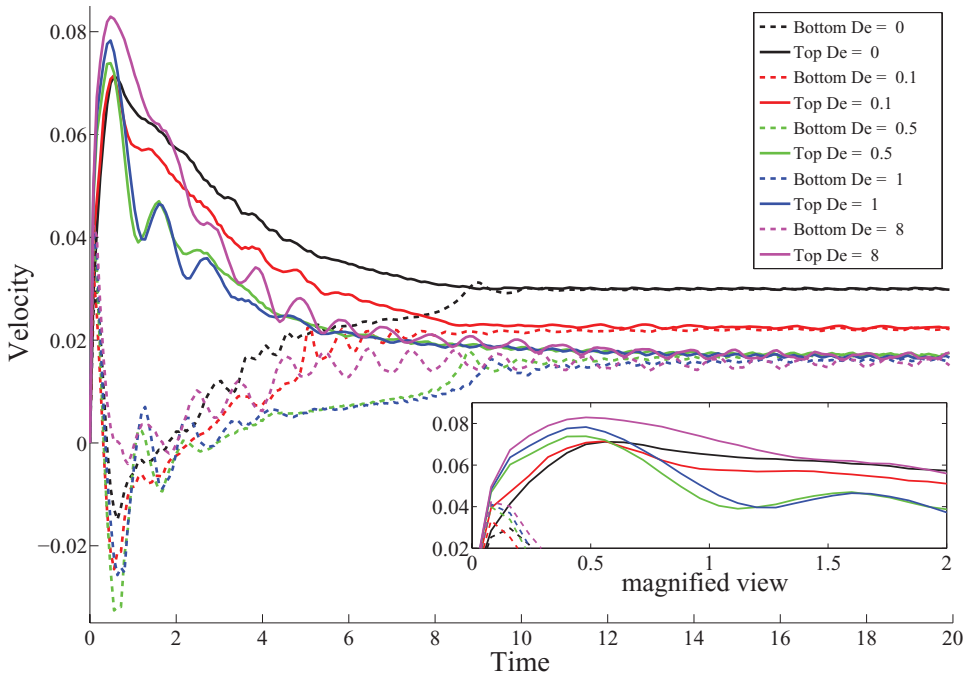

FIG. 6. The swimming speed of the top and bottom sheets over the course of twenty periods of motion as a function of the Deborah number *De*. The inset shows the early transients during the first two periods. We can see that during the first half period, viscoelasticity enhances the velocity differences that ultimately lead to synchronization.

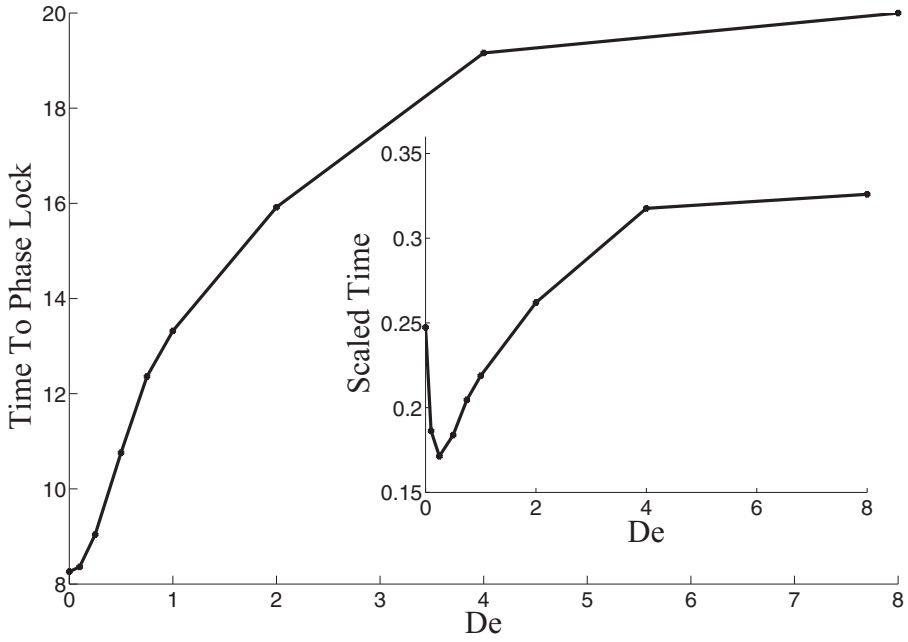

FIG. 7. Time to synchronization as a function of the Deborah number *De*. The sheets were considered phase-locked when the *x*-axis coordinates of the upwardly concave critical points of each sheet were within three-quarters of a mesh spacing. The inset shows the time to synchronization scaled by the time it would take the synchronized pair to swim one body length.

kinematically but are instead determined dynamically through the interaction of the internal stresses of the sheet with the external fluid stresses. These external fluid stresses also capture the interactions between the two sheets, and this interaction is most pronounced at early times in their large and very different departures from the final synchronized shapes.

Another difference from the asymptotic construction of Elfring *et al.*[10] is that we begin from a state of rest for the polymer stress field ($\boldsymbol{\sigma} \equiv \mathbf{0}$) while they construct special solutions to which general initial data will relax on an $O(De)$ time scale (in the small amplitude limit). This allows us to study the temporal development of the viscoelastic stresses, which of course are tightly coupled to the shape dynamics of the sheets. One result that does show some concordance with the Elfring *et al.*[10] analysis is in the early time behavior of the sheet velocities, shown in the inset to Fig. 6. Here we see that viscoelasticity initially enhances the inter-sheet velocity differences that will ultimately lead to synchronization.

The mechanism for phase-locking of these infinite sheets is governed by the difference in velocities of the neighboring sheets. Moreover, as indicated by the asymptotic analysis of Lauga[4] and the computations of Ref. 17, the swimming velocity of an infinite single sheet is a decreasing function of Deborah number. For instance, we can see from Figure 6 that the synchronized velocities in the Newtonian case are about twice those of the sheets swimming at $De = 1$. Due to this inherent time scale that varies with Deborah number, we define the relative time to phase-lock:

$$T_d = T_{pl}/T_s.$$

Here T_s is the time that it would take the two sheets, once they were phase-locked, to swim a single wavelength. This scaled time is shown in Fig. 7(inset). In this measure, the characteristic time to phase lock reaches a minimum, below that of the Newtonian case, at a sub-unity value of De. It is interesting that for this system, which includes sheet-elasticity and fluid inertia, lower viscoelasticity leads to more rapid phase-locking.

B. Interaction of a swimming sheet with other immersed structures

Column 2 of Fig. 3 shows snapshots of the position of an actuated elastic sheet, again immersed in a viscoelastic fluid, as it swims leftward above a passive membrane. This passive membrane has no bending rigidity ($S_c = 0$) but is initially in a stretched state ($|\boldsymbol{X}_s| > 1$) and so behaves as an interface under tension. When unforced, this passive structure will relax to a flat state. In this case its elastic coefficient $S_{I,2}$ is sufficiently small that the passive interface is strongly deformed by motion of the actuated sheet.

A comparison of columns 1 and 2 of Fig. 3 also shows that elastic stresses within the fluid are much smaller for the active-passive pair than for the two actuated sheets. This makes intuitive sense since the passive sheet is much more compliant and its deformability (and mobility) prevents the development of large fluid shear or strain-rates that would stretch the polymer field. These fluidic elastic stresses are illustrated in Fig. 8, again using ellipses to represent the distension of the polymer field. Their deformation from circularity is slight.

While the passive sheet is compliant, it does experience drag from the fluid and so acts as an object against which the active sheet can push itself. From this interaction the passive membrane is pushed slowly rightward by the leftward moving actuated sheet. This results, across a range of Deborah numbers, in an increased speed of locomotion for this active sheet, relative to a single or two active sheets, as is shown in Fig. 11(b). We remark here that this increase in swimming velocity when the sheet is placed next to a passive membrane is also accompanied by a decrease in achieved amplitude (Fig. 11(a)). This will be discussed in more detail in Sec. IV C below.

We now perturb the problem by considering instead a passive bottom sheet that has bending rigidity (i.e., $S_{c,2} > 0$), a zero target curvature $\hat{\kappa}$ (see Eq. (2)), and the same tensile properties as in the previous case. Hence, given the periodic boundary conditions, this passive sheet will again relax, when unforced, to a flat state. As is seen in the third column of Fig. 3, the main effect of this change is that the passive sheet is much more difficult to deform, and it develops very little amplitude

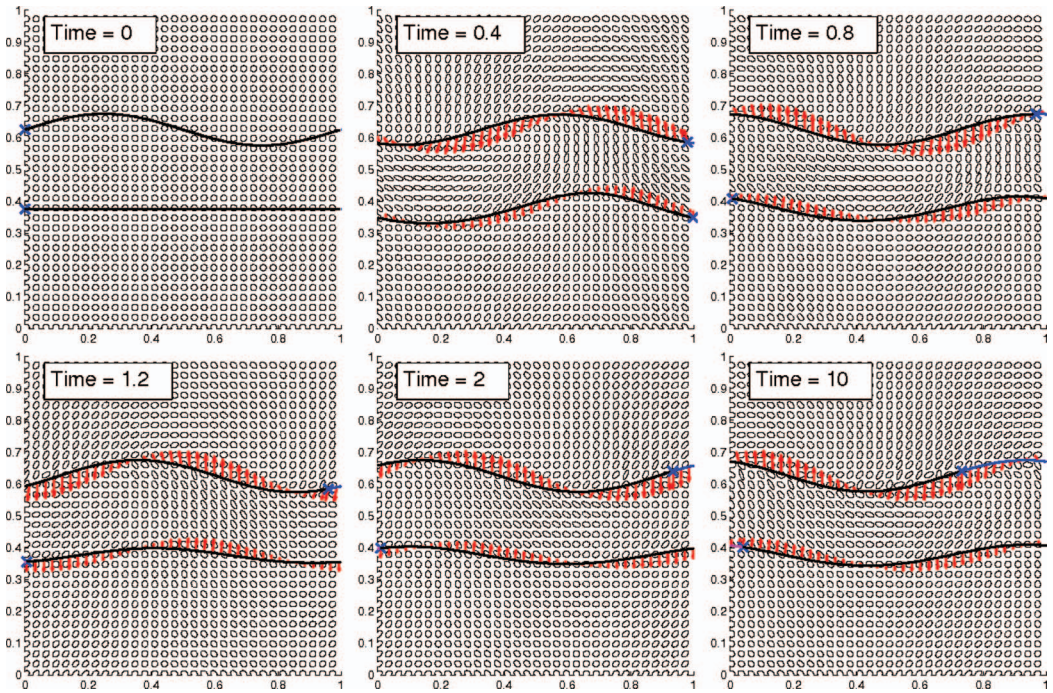

FIG. 8. Snapshots of an actuated sheet above a passive elastic membrane with no bending rigidity. The distension of the polymer field is visualized by ellipses whose axes are in the principle directions of the polymer conformation tensor $\tilde{\boldsymbol{\sigma}}$ with these axes' lengths scaled by the corresponding eigenvalue. Arrows along each filament indicate velocity, and the asterisks, originally placed at the leftmost material points on each filament at time zero, indicate material displacement. Note that while the top, actuated sheet exhibits forward motion to the left, the bottom, passive sheet is actually displaced backward.

of deformation from the passage of the active sheet. This makes perfect sense given that we have increased its overall resistance to bending, and so it should in effect behave as a (nearly) rigid flat wall that is nonetheless mobile. Its relative lack of compliance also leads to greater viscoelastic stresses in the fluids, and these have some rough geometric similarity to those seen in the case of two actuated sheets.

The detailed distension of the polymer field and the velocity field upon the sheets is shown in Fig. 9. As this figure also shows, the passive (but mobile) sheet is again being pushed rightward by the leftward moving active sheet. As in the previous case, Figs. 11(a) and 11(b) show that the active sheet velocity is increased by its interaction with this stiffened passive membrane, being nearly twice as fast as the active sheet pair, even though its achieved amplitude is about 10% less.

Finally, we consider the case of an active sheet moving above a fixed wall. The immersed boundary points of this wall are tethered by strong springs to prescribed spatial positions.[24] The spring constant is chosen large enough so that deviation from these prescribed points is negligible. Snapshots are shown in the fourth column of Fig. 3. The spatial development of viscoelastic stresses is again similar to those of the first and third cases, though little relaxation of these stresses is evident at larger times. The distension of the polymer field is illustrated in Fig. 10, which shows strong stretching both within the bulk, particularly in the area of the minimum height above the wall, and along the active sheet boundaries. Since the wall is immobile against any pushing from the leftward moving sheet, it acts as a superior backstop relative to all other cases, and the active sheet swims considerably faster than any of the other cases (see Fig. 11(b)). The classical problem of Taylor's sheet swimming in a channel bounded by fixed walls was analyzed by Katz[3] using lubrication theory. Katz[3] demonstrated the positive effect of the nearby walls on swimming speed, as we observe here. Locomotion of an actuated sheet next to a wall, using prescribed kinematics, has also been investigated via lubrication theory by Chan *et al.*,[25] as a model for snail locomotion (see also Wilkening and Hosoi[26] for aspects of shape optimization).

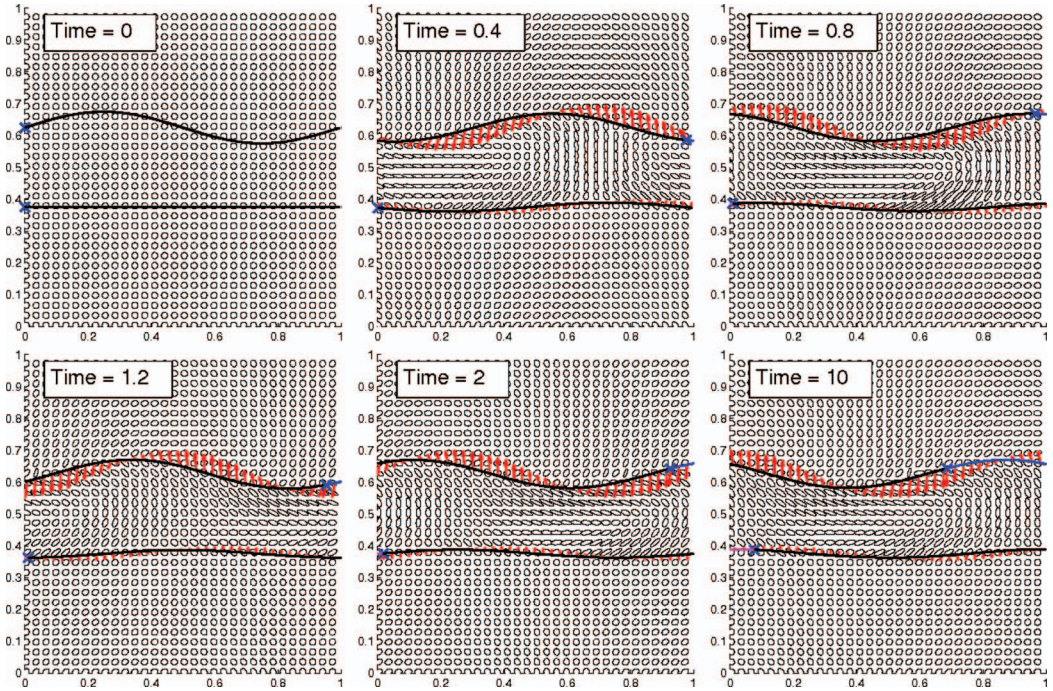

FIG. 9. Snapshots of an actuated sheet above a passive elastic membrane with bending rigidity. The distension of the polymer field is visualized by ellipses whose axes are in the principle directions of the polymer conformation tensor $\tilde{\boldsymbol{\sigma}}$ with these axes' lengths scaled. Arrows along each filament indicate velocity, and the asterisks, originally placed at the leftmost material points on each filament at time zero, indicate material displacement. Note that while the top, actuated sheet exhibits forward motion to the left, the bottom, passive sheet is actually displaced backward.

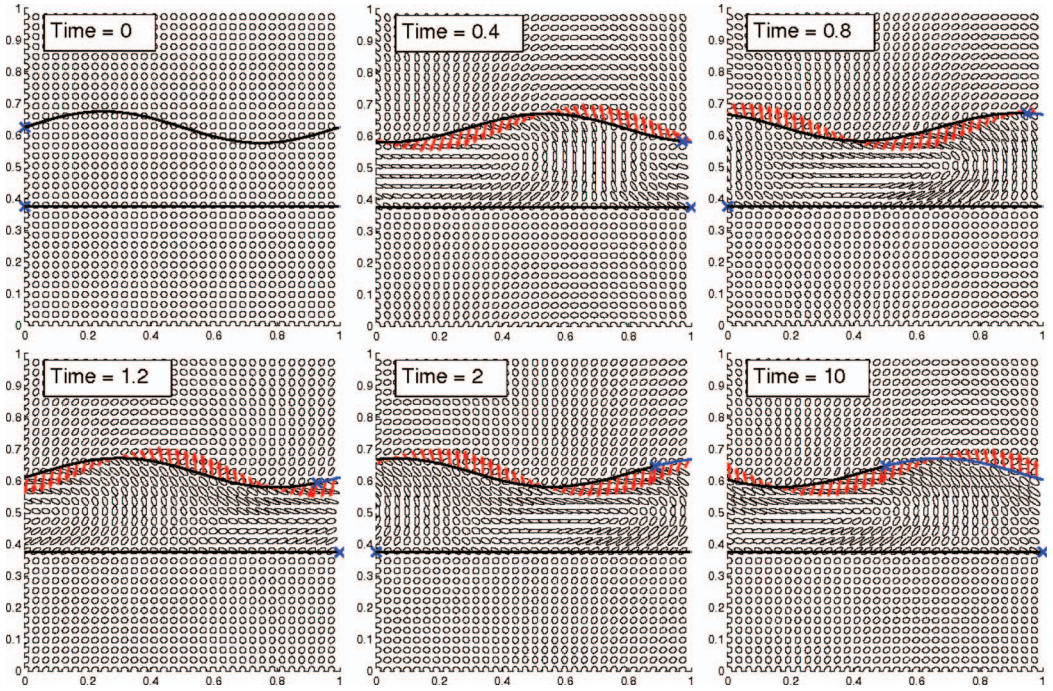

FIG. 10. Snapshots of an actuated sheet above a fixed wall. The distension of the polymer field is visualized by ellipses whose axes are in the principle directions of the polymer conformation tensor $\tilde{\boldsymbol{\sigma}}$ with these axes' lengths scaled. Arrows along each filament indicate velocity, and the asterisks, originally placed at the leftmost material points on each filament at time zero, indicate material displacement. Since the bottom immersed boundary wall is nearly rigid, the asterisk is perturbed only slightly from its initial point, but due to periodic boundary conditions, it appears on each side of the domain.

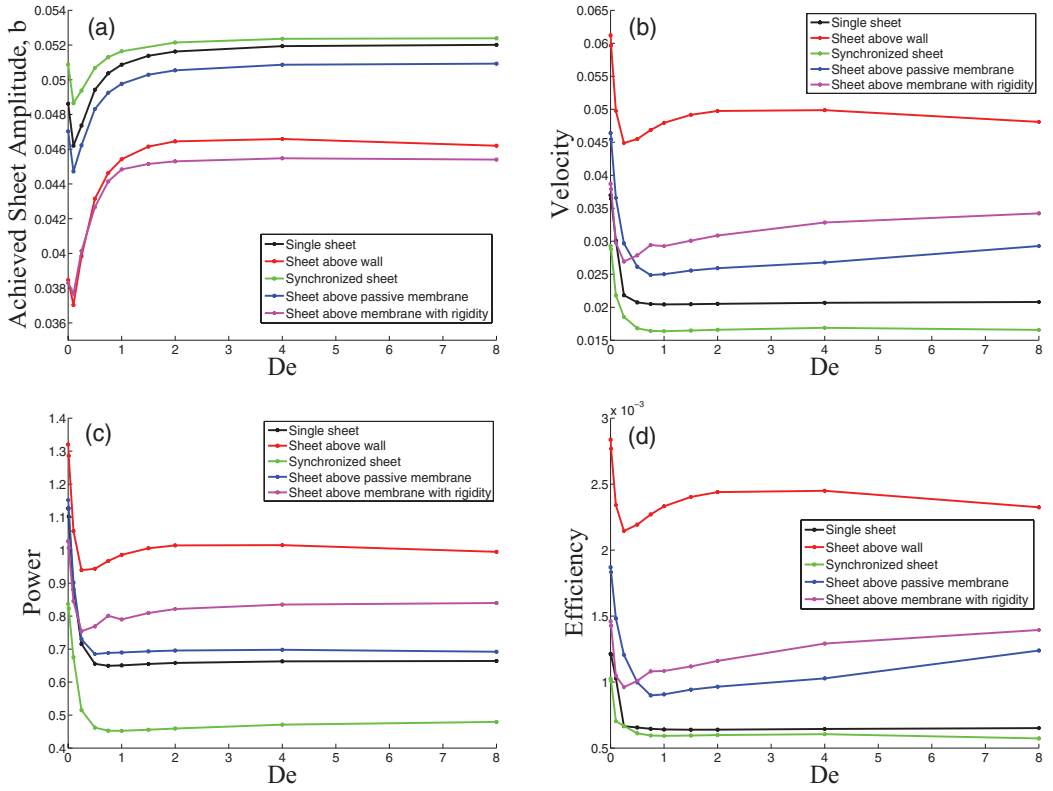

FIG. 11. (a) Achieved amplitude of swimming sheet versus *De*. (b) Average velocity of the top sheet versus *De*. (c) Average power of the top sheet versus *De*. (d) Average efficiency of the top sheet versus *De*.

C. Swimming sheets, their shapes, and their efficiency

Here we compare the shapes, velocities, and efficiencies of the swimming sheets. As a measure of shape, we simply consider the amplitude of the sheet achieved over long times. Figure 11(a) shows this achieved amplitude, while Figure 11(b) shows the corresponding translational velocity found by averaging over the 18th to 20th periods. Here we see that velocity does not correlate positively with amplitude, as Taylor's classical analysis suggests for single swimmers, but rather correlates roughly with proximity to another immersed structure that can be pushed against. That is, the lowest achieved amplitudes and highest velocities are achieved by the sheets swimming next to a mobile, rigid membrane (cyan curve) and a flat, immovable wall (red curve). It is interesting that these two cases also show the largest magnitude of viscoelastic stresses (see columns 3 and 4, respectively, of Fig. 3 at large times). Those stresses are also greatest in the region below the point of minimum sheet amplitude, where the swimming sheet is closest to the underlying structure against which it is pushing. The greater shear in this region is reflected in the large distension of the polymer field there (see Figs. 9 and 10), and this is where normal stresses that push the sheets apart should be greatest. This is likely an important contributor to the decreased sheet amplitude in these two cases, though it is unclear to what degree it affects the swimming velocity.

One measure of the efficiency of swimming is to consider what the average mechanical input power was to achieve the calculated velocity. Obviously, the greater the input power for a given velocity, the less efficient. To this end, a natural dimensionless measure of the mechanical efficiency of swimming by the lth sheet is the ratio:

$$E_{ff} = U_l^2 / \langle P_l \rangle,$$

where $\langle P_l \rangle$ is the time-averaged power input to the fluid by a swimming sheet:

$$\langle P_l \rangle = \frac{1}{(t_1 - t_0)} \int_{t_0}^{t_1} \int_0^1 \boldsymbol{F}_l \cdot \boldsymbol{u}_l ds\, dt. \tag{12}$$

Here $\boldsymbol{F}_l$ is the immersed boundary force given in Eq. (3) for the lth sheet. Typically, there would be a factor of the shear viscosity but this has been set to unity in our nondimensional equations. Further, we are only interested in the relative efficiency between the different sheets, and so neglect the inclusion of constant factors.

Figures 11(c) and 11(d) show the averaged power input and efficiency across Deborah number for the five scenarios considered. Again, these quantities were averaged over the 18th to 20th periods. Here we consider the top sheet ($l = 1$) only. The lowest average input power is achieved by the top sheet of the swimming pair, while the highest is achieved by the single sheet swimming next to the wall. While the sheet next to the wall has the highest input power, it also has a relatively higher speed, and consequently, as Fig. 11(d) shows, the highest mechanical efficiency by a fair measure. In fact, while the advantage of the wall is evident at all De when comparing efficiencies, we see that this advantage is even more pronounced for viscoelastic fluids (De non-zero) than for the Newtonian case.

We may ask how the efficiency in each case varies when we move from a Newtonian fluid ($De = 0$) to a more viscoelastic fluid. We see that for a single swimmer or a pair of synchronized swimmers, the efficiency decreases with De, in agreement with the small amplitude analysis of Lauga,[4] and the simulations of Teran *et al.*,[22] for infinite periodic sheets. However, for swimmers near membranes or walls, we see that there is a range of $De = O(1)$ where efficiency first decreases from the Newtonian case, but then recovers to some intermediate value.

V. CONCLUSIONS

Here we have investigated the dynamics of an actuated elastic sheet immersed in a viscoelastic fluid interacting with neighboring structures. We have demonstrated that a neighboring wall or membrane with bending rigidity enhances the efficiency of a swimming sheet, and that this enhancement increases with Deborah number. In addition, we have captured the spatial development and relaxation of viscoelastic stresses between two actuated sheets as they synchronize.

Here we have chosen the Oldroyd-B model which, while highly idealized, does capture elastic responses and the generation of normal stresses found in many complex fluids. However, it would be very interesting to re-examine the dynamics of an actuated sheet interacting with immersed structures using more nonlinear fluid models, such as the Giesekus or FENE-P models, that capture effects such as shear-thinning or the finite distension of polymer strands.

We emphasize that we have chosen to consider only the classical swimming sheet of infinite extent. While much insight can be gained from this system, we caution against the overzealous extrapolation of the results of this idealized geometry to real biological systems or even two-dimensional model swimmers of finite extent. The dramatic process of flagellar attraction depicted in the experiments of Woolley *et al.*[12] cannot be studied in this restrictive context because the incompressibility of the fluid between the infinite sheets would allow no such attraction. Moreover, while it has been shown both analytically and computationally that viscoelasticity hampers the swimming speed of Taylor's infinite sheet,[4,17] computations show that finite two-dimensional filaments with accentuated tail amplitude exhibit a boost in swimming speed when the frequency of actuation is tuned to the viscoelastic fluid's polymer relaxation time.[17] This is a prime example illustrating that details of individual systems could trump unifying principles—recent experiments show that *C. elegans*, who swim with a large, constant amplitude gait, maintain the same kinematics in more viscoelastic environments, but swim more slowly as viscoelasticity increases.[27] Lastly, as yet another example of the importance of details, Liu *et al.*[28] have demonstrated experimentally that model helical swimmers can achieve maximal speed and efficiency in a simple viscoelastic fluid when $De = O(1)$.

ACKNOWLEDGMENTS

The work of J.C. and L.F. was supported in part by National Science Foundation (NSF) (Grant No. DMS-0652795). The work of M.S. was supported in part by NSF (Grant No. DMS-0652775) and (U.S.) Department of Energy (DOE) (Grant No. DE-FG02-88ER25053).

[1] G. Taylor, "Analysis of the swimming of microscopic organisms," Proc. R. Soc. London, Ser. A **209**(1099), 447–461 (1951).
[2] E. Lauga and T. Powers, "The hydrodynamics of swimming microorganisms," Rep. Prog. Phys. **72**, 096601 (2009).
[3] D. Katz, "On the propulsion of micro-organisms near solid boundaries," J. Fluid Mech. **64**, 33 (1974).
[4] E. Lauga, "Propulsion in a viscoelastic fluid," Phys. Fluids **19**(8), 083104 (2007).
[5] A. Leshansky, "Enhanced low-Reynolds-number propulsion in heterogeneous viscous environments," Phys. Rev. E **80**, 051911 (2009).
[6] H. Fu, V. Shenoy, and T. Powers, "Low-Reynolds-number swimming in gels," Europhys. Lett. **91**, 24002 (2010).
[7] L. Fauci, "Interaction of oscillating filaments: A computational study," J. Comp. Phys. **86**, 294–313 (1990).
[8] G. Elfring and E. Lauga, "Hydrodynamic phase locking of swimming microorganisms," Phys. Rev. Lett. **103**, 088101 (2009).
[9] G. Elfring and E. Lauga, "Passive hydrodynamic synchronization of two-dimensional swimming cells," Phys. Fluids **23**, 011902 (2011).
[10] G. Elfring, O. Pak, and E. Lauga, "Two-dimensional flagellar synchronization in viscoelastic fluids," J. Fluid Mech. **646**, 505–515 (2010).
[11] S. A. House, D. J. Richter, J. K. Pham, and S. C. Dawson, "*Giardia* flagellar motility is not directly required to maintain attachment to surfaces," PLoS Pathog. **7**(8), e1002167 (2011).
[12] D. Woolley, R. Crockett, W. Groom, and S. Revell, "A study of synchronisation between the flagella of bull spermatozoa, with related observations," J. Exp. Biol. **212**, 2215 (2009).
[13] J. Sznitman, P. Purohit, P. Krajacic, T. Lamitina, and P. Arratia, "Material properties of *caenorhabditis elegans* swimming at low Reynolds number," Biophys. J. **98**, 617 (2010).
[14] S. Jung, "*Caenorhabditis elegans* swimming in a saturated particulate system," Phys. Fluids **22**, 031903 (2010).
[15] T. Majmudar, E. Keaveny, J. Zhang, and M. Shelley, "Experiments and Theory of Undulatory Locomotion in a Simple Structured Medium," J. R. Soc., Interface **9**, 1809–1823 (2012).
[16] G. Elfring and E. Lauga, "Synchronization of flexible sheets," J. Fluid Mech. **674**, 163–173 (2011).
[17] J. Teran, L. Fauci, and M. Shelley, "Viscoelastic fluid response can increase the speed and efficiency of a free swimmer," Phys. Rev. Lett. **104**, 038101 (2010).
[18] R. Bird, R. Armstrong, and O. Hassager, *Dynamics of Polymeric Liquids* (Wiley, New York, 1987).
[19] R. Larson, *The Structure and Rheology of Complex Fluids* (Oxford University Press, Oxford, 1998).
[20] C. S. Peskin, "The immersed boundary method," Acta Numerica **11**, 479–517 (2002).
[21] J. Chrispell, R. Cortez, D. Khismatullin, and L. Fauci, "Shape oscillations of a droplet in an Oldroyd-B fluid," Physica D **240**, 1593 (2011).
[22] J. Teran, L. Fauci, and M. Shelley, "Peristaltic pumping and irreversibility of a Stokesian viscoelastic fluid," Phys. Fluids **20**(7), 073101 (2008).
[23] E. O. Tuck, "A note on a swimming problem," J. Fluid Mech. **31**, 305–308 (1968).
[24] H. Williams, L. J. Fauci, and D. P. Gaver, "Evaluation of interfacial fluid dynamical stresses using the immersed boundary method," Discrete Contin. Dyn. Syst., Ser. B **11**, 519–540 (2009).
[25] B. Chan, N. Balmforth, and A. Hosoi, "Building a better snail: Lubrication and adhesive locomotion," Phys. Fluids **17**, 113101 (2005).
[26] J. Wilkening and A. Hosoi, "Shape optimization of a sheet swimming over a thin liquid layer," J. Fluid Mech. **601**, 25–61 (2008).
[27] X. Shen and P. Arratia, "Undulatory swimming in viscoelastic fluids," Phys. Rev. Lett. **106**, 208101 (2011).
[28] B. Liu, T. Powers, and K. Breuer, "Force-free swimming of a model helical flagellum in viscoelastic fluids," Proc. Natl. Acad. Sci. U.S.A. **108**, 19516 (2011).